D2.3
In-situ bulk measurements

General information	
Grant agreement number	755500
Start date of the project	01/09/2017
Project duration	54 months
Due date of the deliverable	31/08/2021
Actual submission date	24/02/2022
Lead beneficiary	KTU

Keywords
In-situ bulk measurements

Type	Meaning	
R	Document, report	x
DEM	Demonstrator, pilot, prototype	
DEC	Websites, patent fillings, videos, etc.	
OTHER	Software, technical diagram, etc.	

Dissemination Level		
PU	Public	x
CO	Confidential, only for members of the consortium (including the Commission Services)	

Table of Contents

Table of Tables

Table of Figures

1 Executive Summary

This deliverable reports results obtained at WP2 T2.3 – Measurement of bulk material properties. It focuses on average grain size evaluation of cast components and presents two approaches based on the Stanke Kino (SK) model and two point correlation function (TPCF). The considered approaches are based on attenuation measurements and allows to get both indicative grain size estimation and to evaluate the grain distribution across the inspected volume. The report summarizes the most important concepts and limitations of the presented approaches, which are supported with numerical, experimental examples and confirmed with Electron backscatter diffraction (EBSD) characterisations.

The first part of the document presents average grain size estimation technique based on the Stanke Kino model, which can provide an indicative value of the grain size. This approach is first confirmed with the synthetic microstructural models and later with different cast components from the Advise project repository. To eliminate the errors of the attenuation measurement, the measurement procedure is confirmed on materials with well defined properties and with the sensitivity analysis. Despite that the majority of the investigated samples were not characterised at the particular positions, where the attenuation has been measured, the overall grain size values were found to be in good agreement with the available metallography data.

The second part of the report discusses the non-uniqueness of the attenuation measurement for different grain size distribution to mean ratios. This part is based on the recently published paper and presents an approach for mean grain size evaluation which considers grain size distribution. The technique is demonstrated on the sample of Advise inventory, which was characterised at attenuation measurement positions. In general, good agreement was found between the linear correlation length obtained from attenuation measurements and metallography. It was found that a single exponential fit may underestimate the areas with large grains as these quite essentially dominate the measured attenuation.

Finally, the report concludes by presenting benefits and limitations of each approach and indicates subjects of the future research.

2 Introduction

Nuclear power plant (NPP) regulations require to ensure safety of critical components by means of non-destructive testing and qualified inspection procedures that has proven ability to detect certain defects. However, coarse grained materials and castings commonly found in nuclear installations, including the primary coolant piping system in pressurised water reactors, significantly degrade the performance of ultrasonic inspection techniques. This is due to microstructures with large grains, inducing scattering of the ultrasonic waves at grain boundaries, which is responsible for both structural noise and attenuation. Hence, the inspection depth is limited by backscatter of the signal from grain boundaries and scattering related attenuation. Moreover, local variations of the material characteristics due to solidification kinetics, in particular grain size and crystal orientation, lead to different ultrasonic responses at different transducer positions. These factors significantly complicate qualification and validity of inspection procedures. Apparently the procedure has to cover typical range of grain sizes and their distributions for each given component. However, qualification procedures usually rely on mock-ups, so the correspondence to on site components cannot be guaranteed. This in particular concerns cast mockups which essentially differ from welds, as the manufacturing procedure is less controlled and monitored. Due to abovementioned reasons site operators need tools to evaluate grain properties on site so they are able to confirm, that the component under inspection has similar properties to the mock-up used for qualification.

This report presents joint effort between EDF, ICL and KTU in WP2, T2.3 related to grain size evaluation in bulk materials. The techniques presented in this deliverable can be arranged in two groups. First, a metric to evaluate average grain size from attenuation measurement is presented which is based on the Stanke-Kino model and is valid for homogenous structures with equiaxed grains. This approach was developed and tested by KTU. Second, a more sophisticated metric based on a two-point correlation function is presented that was developed by Imperial College London and takes into account the grain distribution. First technique is devoted for rough grain size estimation and can give general idea of the grain sizes in the structure when the operator is not concerned at grain size estimation with accuracy of tens of microns. As it will be shown later, attenuation measurement can be non-unique when one distribution is with a large mean and small standard deviation-to-mean ratio and the other one with a small mean and large standard deviation-to-mean ratio. This is important for precise grain size evaluation or in case of samples with essentially different grain distributions. Nevertheless, second technique based on two-point correlation function can be used for such cases. The part of the work concerning technique based on two-point correlation function had been published in Ultrasonics[1].

[1] Y. Liu, M.K. Kalkowski, M. Huang, M.J.S. Lowe, V. Samaitis, V. Cicėnas, A. Schumm, Can ultrasound attenuation measurement be used to characterise grain statistics in castings?, Ultrasonics, Volume 115, 2021.

3 Average grain size estimation based on SK model

Elastic waves in polycrystalline media are scattered at grain boundaries, while the acoustic energy is distorted, attenuated and diffused. The attenuation is caused by diminishing amplitude of the wave propagating through component due to scattering at grain boundaries. In backscatter, the waves that were reflected at grain boundaries can be captured in pulse-echo measurement. While backscatter is considered to be the method of choice for determining local grain characteristics, in this report we use frequency dependent elastic wave attenuation as a primary tool for evaluation of grain statistics in castings. The choice was determined by the observed better attenuation sensitivity to the variation of the local grain structure, at least for the particular cases that were analysed. In the few following paragraphs, the average grain size estimation technique, based on Stanke-Kino model will be briefly described and validated with simulations and experiments. The proposed technique implicitly assumes that the structure is homogeneous, untextured, while the grains are equiaxed and normally distributed.

3.1 Description of average grain size estimation method

The proposed average grain size estimation technique of bulk materials is based on the measurement of frequency dependent attenuation and fitting the result to a family of theoretically estimated Stanke Kino (SK) curves[2,3] by minimizing the cost function:

$$a_{est} = \arg\left\{ \min_{a_n} \left[\left(\lg(\alpha_L(f, a_n)) - \lg(a_{\exp}(f)) \right)^2 \right] \right\}, \tag{3.1}$$

where $\alpha_L(f,a_n)$ is a family of SK curves, a_n is average grain size value, n=1÷N; N is the total number of grain sizes used. A summarized procedure of average grain size estimation can be illustrated with Fig. 3.1.

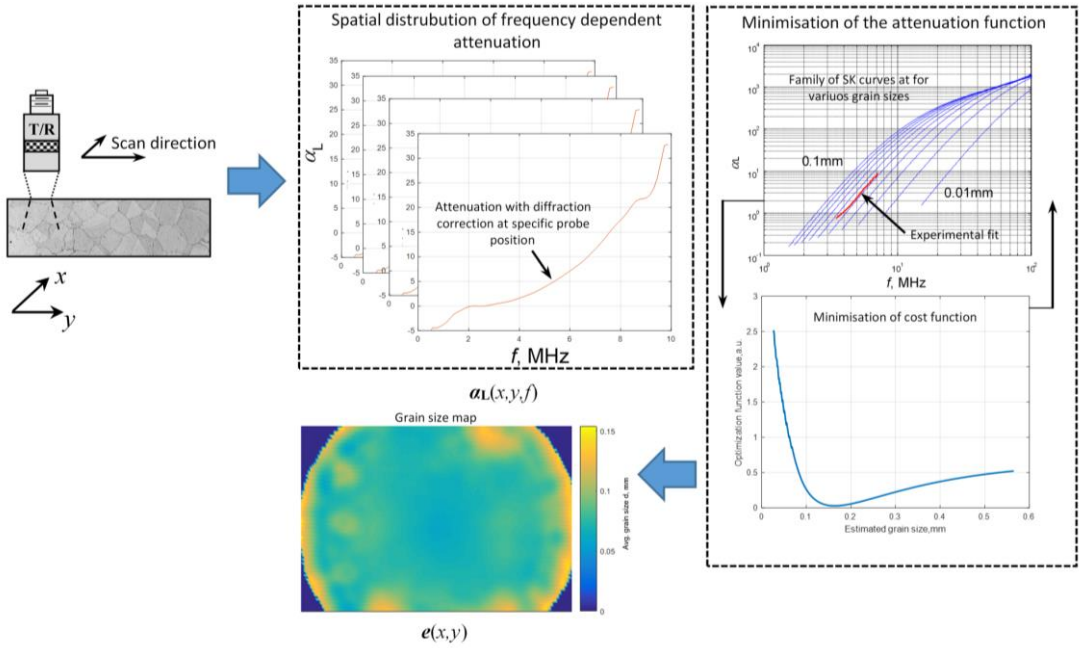

Figure 3-1. Illustration of average grain size estimation approach using a SK model

[2] F.E. Stanke, G.S. Kino, "A unified theory for elastic wave propagation in polycrystalline materials", J. Acoust. Soc. Am. 75, 665-681 (1984).

[3] Van Pamel, G. Sha, M.J.S. Lowe, S.I. Rokhlin, "Numerical and analytical modelling of elastodynamic scattering within polycrystalline materials", J. Acoust. Soc. Am. 143 (4), 23942408 (2018).

To keep the report brief, the detailed procedure of grain size estimation is presented in the Annex 6. The selected approach based on SK model is valid for untextured polycrystals with cubic symmetry, uniform grain size distribution and assumes that scatterers are equiaxed. The model considers single-scattering at grain boundaries and has been validated in Rayleigh and stochastic scattering regions.

3.2 Verification of the approach on a synthetic microstructure

To evaluate the performance of proposed grain size estimation technique, synthetic microstructure models were created first, which allow to control the statistics of grains. The simulations were computed for two grain averages – 500 µm and 1000 µm and the reconstructions of the mean grain size were conducted with the proposed model.

3.2.1 Model description

The chosen geometry of the synthetic microstructure model was a cuboid 12 × 12 × 100 mm. Grains were generated using a Voronoi tessellation algorithm embedded in *Neper*[4], where the specified number of grains dictates the average grain size. The material of interest is Inconel and the investigation focused on longitudinal waves only.

For this study, the results were computed for two average grain sizes - 500 µm and 1000 µm, where for the chosen geometry, the desired average grain sizes correspond to 115200 and 14400 Voronoi grains, respectively. The calculations were executed on a graphical processing unit (GPU) using Pogo solver developed at Imperial College London[5]. This simulation process had been validated by previous studies[3]. The parameters of the simulation are listed in the Table 3.1 below.

Table 3-1. The parameters of the Neper models used in simulations

Model variant	*Dimensions* (mm)	*Average grain size* (mm)	*No of Voronoi grains*	*Mesh size* (mm)	*No of DoFs* ($\times 10^6$)	*Centre frequencies* (MHz)
1	12 × 12 × 10 mm	1	14400	0.1	44	0.2 – 2, 0.2 step
2	12 × 12 × 10 mm	0.5	115200	0.05	349	0.25 – 3, 0.25 step

The computation was thought to deliver attenuation profiles as a function of the wavenumber-length scale product, where the length scale corresponds to the average grain size (equivalent diameter) *d*. We assumed that the material is non-textured and crystals are randomly oriented. Equivalent grain sizes generated by *Neper* are plotted below in Figure 3.2. The desired average grain size values are denoted with red lines.

3.2.2 Results

The example of SK curve obtained for average grain sizes of 500 µm and 1000 µm is presented in Fig. 3.3. It can be observed, that the flat zone of ambiguity exists at frequencies above 1.5 MHz, where two SK curves overlap. This is an important zone to consider, as measurements at such frequencies may lead to grain size estimation errors. In practice, such zone of ambiguity is mostly important for grains with large sizes.

[4] Quey R., Dawson P.R., Barbe F. Large-scale 3D random polycrystals for the finite element method: Generation, meshing and remeshing. Comput. Methods Appl. Mech. Engrg., 200 (2011), pp. 1729-1745

[5] Huthwaite P. Accelerated finite element elastodynamic simulations using the GPU. J. Comput. Phys., 257 (2014), pp. 687-707

The reconstructed average grain sizes at different excitation frequencies for 500 µm and 1000 µm models are presented in Fig. 3.4. From the results it can be observed that reconstruction accuracy is frequency dependent, showing that the best reconstruction frequency for 500 µm case is 1.75 MHz, while for 1000 µm it is 1 MHz. The reconstruction error increases with higher frequencies which is a consequence of the overlap zone. On average, the estimated grain size for 500 µm is 467 µm, while for 1000 µm model it is 1097 µm.

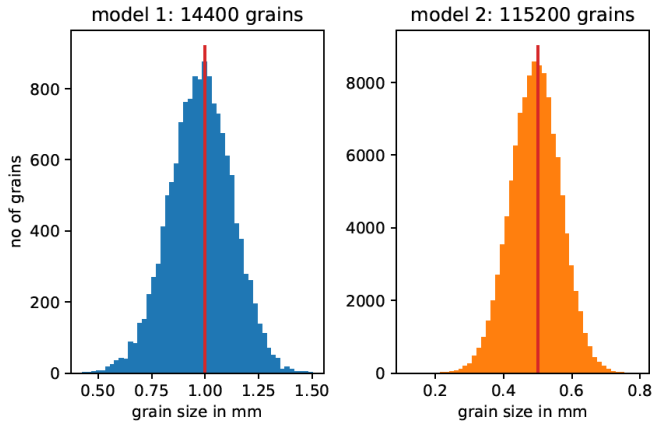

Figure 3-2. Equivalent grain sizes generated by *Neper* model, where red lines denote average grain size

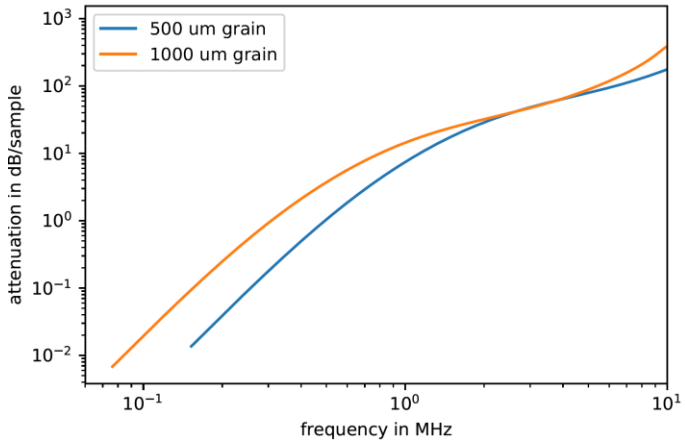

Figure 3-3. SK curve obtained using *Neper* model with different average grain sizes

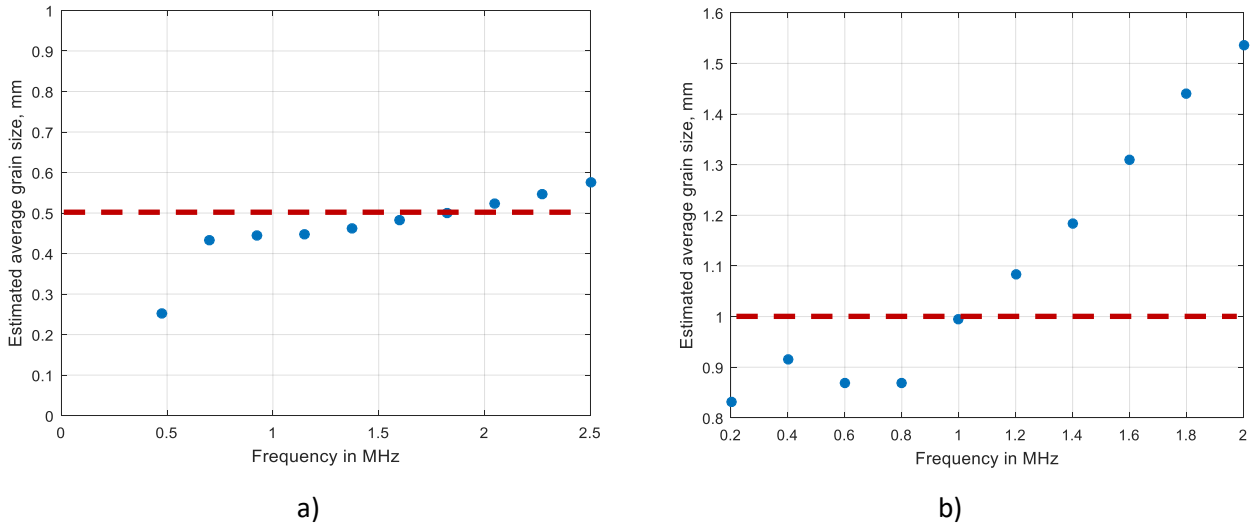

a) b)

Figure 3-4. Reconstructed average grain size from *Neper* model at different excitation frequencies: model with 0.5 mm average grain size (a), model with 1 mm average grain size (b)

3.3 Experimental verification of approach on representative mock-ups

In this section the average grain size estimation technique is verified with experiments on representative samples from the Advise mock-up repository. In total, 6 mock-ups were selected, owned by EDF and Framatome. First, the mock-ups used in this task are briefly described, followed by attenuation measurement procedure and average grain size reconstruction results.

3.3.1 Description of selected relevant mock-ups

The summary of the mock-ups used for experimental verification of average grain size estimation technique is presented in Table 3.2. The schematic drawings of the selected mock-ups are presented in the annex 7. Mock-ups 1618-B359-B1, B359-2 and 1618-B359-B3 are chromium-nickel-based alloy (Inconel600) samples harvested from a forged bar representative of the heads of reactor vessel (see Fig. 3.5). Block 1618-B359-B1 remained in initial state, while other blocks B359-2 and 1618-B359-B3 underwent a thermal treatment in order to modify their microstructure. Three different average grain sizes were obtained, which are listed in Table 3.6. The metallographic analysis was performed for the mock-ups from a slice with dimensions of 20×20×8 mm^3 located at the heart of the sample. The obtained grain size distributions are presented in Fig. 3.9. The mock-ups 1618-B359-B1, B359-2 and 1618-B359-B3 are assumed to be homogeneous, with equiaxed grains and no texture.

Table 3-2. Mock-ups used for experimental verification of grain size estimation technique

Mock-up reference	*Dimensions* (mm)	*Average grain size* (µm)	*Material*	*Mock-up owner*
1618-B359-B1	90 × 90 × 284 mm	89.2	Inconel600	EDF
B359-2	90 × 90 × 324 mm	288	Inconel600	EDF
1618-B359-B3	90 × 90 × 284 mm	748	Inconel600	EDF
RDIM3	398 × 110 mm	300 - 2400	Stainless steel	Framatome
1591-B359-D2	Phi=153, h=100 mm	unknown	Inconel600	EDF
1591-B359-D3	Phi=153, h=100 mm	50 - 70	Inconel600	EDF

a) b) c)

Figure 3-5. Chromium-nickel alloy samples used for average grain size measurements: 1618-B359-B1 (a), B359-2 (b) and 1618-B359-B3 (c)

The RDIM3 mock-up is a segment of a pipe with radius of 400 mm. It has a coarse grained homogenous structure of 18 % fine grain (average grain index 0.5, diameter = 0.3 mm) in a matrix of 82 % coarse grain (average grain index -5.5, diameter = 2.4 mm). The image of the mock-up is presented in Fig. 3.7.

The mock-ups 1591-B359-D2 and 1591-B359-D3 possess about 135 mm diameter and 100 mm height which were cut out of a cylindrical cast Inconel 600 slab. The sections underwent heat treatment with the effect of increasing grain size through the merging of smaller grains. This series of mock-ups was intended to serve as laboratory mock-ups to evaluate backscatter and attenuation of ultrasonic waves. According to the manufacturing procedure and previous measurements at EDF's laboratories, the mock-up is assumed to be homogeneous in a macroscopic sense, with approximately equiaxed grains and no texture. It does not exhibit a layered structure with different grain sizes. The mock-ups are illustrated at Fig. 3.8. Mock-up 1591-B359-D3 was characterized with metallographic analysis at three different positions on the surface of sample, estimating the average grain size of 51.9 µm, 66.8 µm and 60.1 µm. The detailed characterization procedure is described in chapter 4.1.2. The histograms of equivalent grain diameters for three characterization zones are presented in chapter 4, Fig. 4.3.

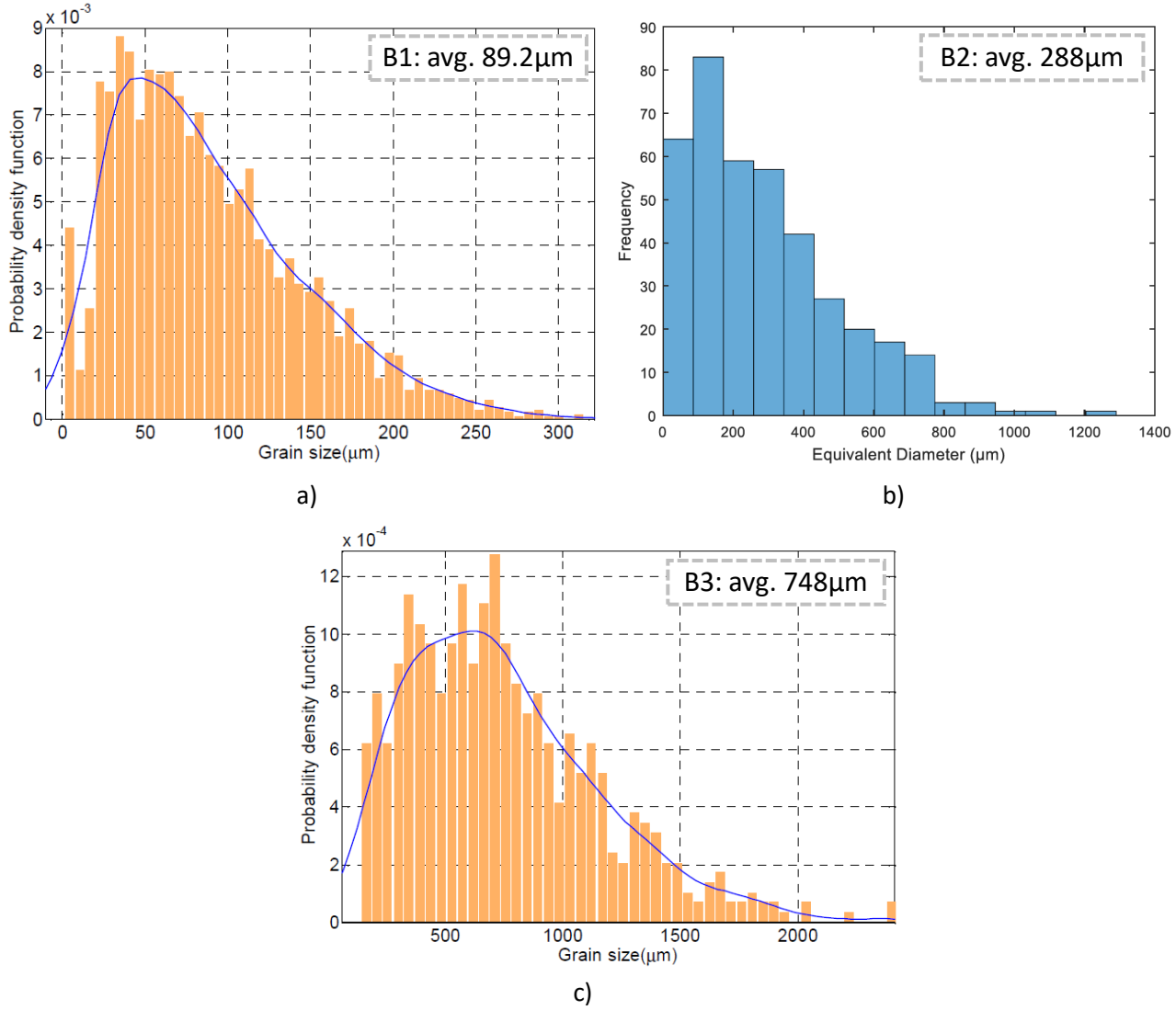

Figure 3-6. Grain size distributions of mock-ups 1618-B359-B1 (a), B359-2 (b) and 1618-B359-B3 (c)

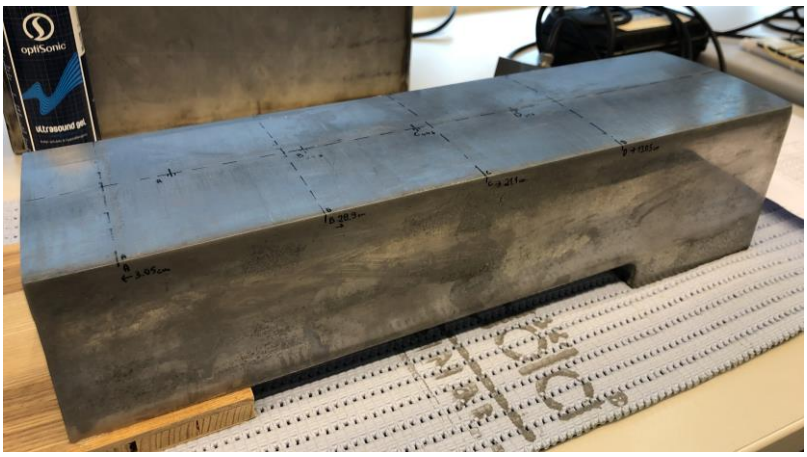

Figure 3-7. Mock-up RDIM3 – a stainless steel segment of a pipe with radius of 400 mm

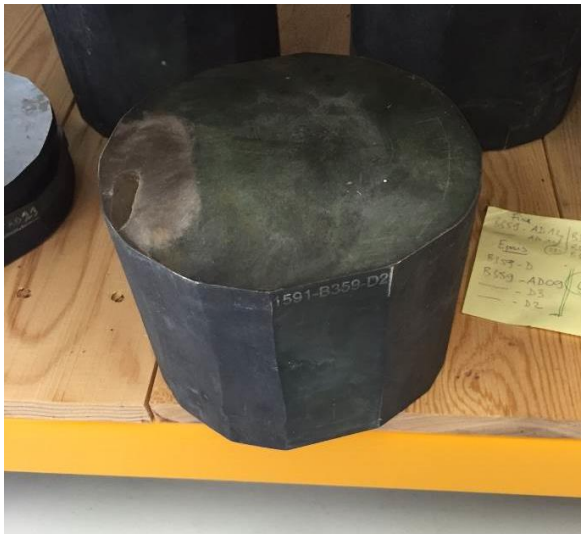

a)

b)

Figure 3-8. Chromium-nickel alloy samples used for average grain size measurements: 1591-B359-D2 (a), 1591-B359-D3 (b) and 1591-B359-D4 (c)

3.3.2 Description of experimental attenuation measurement procedure

The attenuation across the sample described in the previous subsection was measured experimentally. For the sake of better accuracy and confidence in the results, the measurements were taken in an immersion tank using two configurations: pulse-echo (PE) and through-transmission (TT). In practice, the through-transmission setup can be considered as the more reliable approach, as it is less affected by the geometry and the uneven surface of the mock-up than a pulse-echo technique. In this section, the measurements for both PE and TT approaches are presented and compared, however, in the subsequent sections, we only use the data from the PE measurement, as it is more representative of a real in-situ scenario.

A schematic diagram of the measurement set-up is shown in Fig. 3.9. For pulse-echo measurements, the transducer T1 (Olympus C326-SU) was used to collect signals reflected from front-wall $P_{r1}(t)$ and back wall $P_{r2}(t)$ of the mock-up. In the through-transmission approach, another sensor T_2, with same model and characteristics as T_1, was introduced to collect the water path signal without the presence of the specimen $P_w(t)$ and the signal propagated through the mock-up $P_{t1}(t)$. In both cases, the transducers were scanned across the *x-z* plane with the scan step of 1mm covering the entire volume of the specimen. The transducers

T_1 and T_2 were 0.375-inch flat face probes operating at the frequency of 5 MHz with the bandwidth of 56.33 % at -6 dB level. The positions of the sensors must be selected to position the mock-up in the far-field and to avoid the overlap of the reflected and transmitted signals in the time domain.

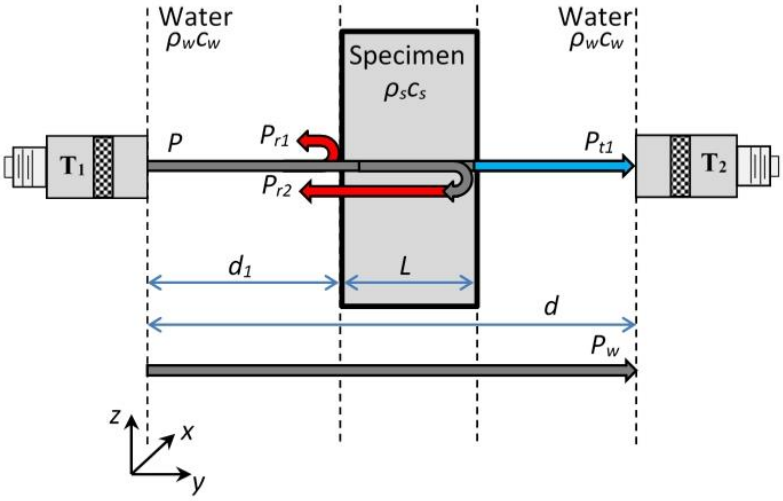

Figure 3-9. Attenuation measurement setup with the arrangements for PE and TT measurements

After the acquisition, the frequency-dependent attenuation was calculated at each scanning position. The material properties of both the mock-up and water were assumed for subsequent calculations, as follows: c_s=5800 m/s; ρ_s=8290 kg/m^3; c_w=1482 m/s; ρ_w=1000 kg/m^3. For the pulse-echo measurement, the attenuation coefficient was calculated from the front wall and back wall reflected signal amplitude spectra:

$$|U_{r1}(f)| = |U_0(f) \cdot R_{ws}| e^{-2 \cdot \alpha_w(f) \cdot d_1}, \tag{3.2}$$

$$|U_{r2}(f)| = |U_0(f) \cdot (-R_{ws}) \cdot T| e^{-2 \cdot \alpha_w(f) \cdot d_1 - 2 \cdot \alpha(f) \cdot L}, \tag{3.3}$$

where $U_{r1}(f)$ and $U_{r2}(f)$ are the Fourier transforms of the measured time histories $P_{r1}(t)$ and $P_{r2}(t)$, $U_0(f)$ is the Fourier transform of initial pulse $P_0(t)$ launched by transducer, f is frequency, R_{ws} is the reflection coefficient at the water-specimen interface, $\alpha_w(f)$ is the attenuation in water, d_1 is the distance between the transducer and the specimen, T is the transmission coefficient, $\alpha(f)$ is the attenuation in the specimen, and L is the thickness of the specimen. The reflection coefficient R_{ws} is defined as:

$$R_{ws} = \frac{z_s - z_w}{z_s + z_w} \tag{3.4}$$

where the water and specimen characteristic acoustic impedances are $z_w = \rho_w c_w$ and $z_s = \rho_s c_s$, respectively. The transmission coefficient T represents the loss of amplitude when propagating across both the water-specimen and the specimen-water interfaces:

$$T = \frac{4 \cdot z_s \cdot z_w}{(z_s + z_w)^2} \tag{3.5}$$

where we note that $T = 1 - R_{ws}^2$.

In the case of the through-transmission measurement, the attenuation coefficient was obtained from the signal transmitted through the water without the specimen, $P_w(t)$, and the signal transmitted through the immersed specimen, $P_{t1}(t)$. The Fourier transforms of the respective signals can be written as:

$$|U_{t1}(f)| = |U_0(f) \cdot T| e^{-\alpha_w(f) \cdot (d-L) - \alpha(f) \cdot L}, \tag{3.6}$$

$$|U_w(f)| = |U_0(f)| e^{-\alpha_w(f) \cdot d}, \tag{3.7}$$

where d is the distance between transducers, $U_{t1}(f)$ and $U_w(f)$ are the Fourier transforms of the measured time histories $P_{t1}(t)$ and $P_w(t)$. To achieve high accuracy with finite size transducers, the diffraction correction must be applied. This was done following[6]:

$$D_i(f) = 1 - \exp\left[-j\frac{2\pi}{s_i(f)}\right]\left[J_0\frac{2\pi}{s_i(f)} + jJ_1\frac{2\pi}{s_i(f)}\right] \tag{3.8}$$

where j is the imaginary unit, J_0, J_1 are the Bessel function of the 0th and the 1st order, respectively, and the subscript i indicates the wave path.The arrangements considered in this report are governed by four different wave paths (referring to Fig. 3.9), so four s_i parameters are needed:

$$s_{r1}(f) = \frac{2d_1c_w}{fr^2}, \tag{3.9}$$

$$s_{r2}(f) = \frac{2d_1c_w}{fr^2} + \frac{2Lc_s(f)}{fr^2}, \tag{3.10}$$

$$s_w(f) = \frac{dc_w}{fr^2}, \tag{3.11}$$

$$s_{t1}(f) = \frac{(d-L)c_w}{fr^2} + \frac{Lc_s(f)}{fr^2}, \tag{3.12}$$

where r is the active radius of the transducer.

The attenuation coefficients for both measurement configurations were calculated from the reflected and transmitted signals, and including the correction factors outlined above, using the following expressions:

$$\alpha_{PE}(f) = \frac{1}{2L}\left[\ln\left(\frac{|U_{r1}(f)|}{|U_{r2}(f)|}\right) - \ln\left(\frac{|D_{r1}(f)|}{|D_{r2}(f)|}\right) + \ln(|1-R_{ws}^2|)\right], \tag{3.13}$$

$$\alpha_{TT}(f) = \frac{1}{2L}\left[\ln\left(\frac{|U_w(f)|}{|U_{t1}(f)|}\right) - \ln\left(\frac{|D_w(f)|}{|D_{t1}(f)|}\right) + \ln(|1-R_{ws}^2|)\right]. \tag{3.14}$$

3.3.3 Validation of the attenuation measurement technique on plexiglass mock-up

The aim of this section was to verify the attenuation measurement techniques on the samples with well-known characteristics. For this purpose, a 20 mm plexiglass sample has been selected. The measurements were taken in pulse-echo and through-transmission set-ups according to the description presented in previous chapter at 5MHz. In practice, the through-transmission setup can be considered as the more reliable approach, as it is less affected by the geometry and diffraction than a pulse-echo technique. The reconstructed attenuation then was compared with a reference curve, published by Zhao et al. (2005)[7]. The results are presented in Fig. 3.10. The "a" part of the figure shows pulse-echo measurements without and with diffraction correction, while "b" part demonstrates comparisons between corrected pulse-echo and through transmission measurements. The red dashed line represents a linear approximation of the estimated attenuation. The slight mismatch can be observed between our measurements and results publish by Zhao et al. at frequencies below 2 MHz. This is due to the bandwidth of the 5MHz transducer used in the experiments which is 60 % at –6 dB (bandwidth 2 MHz – 8 MHz).

[6] Rogers P.H., Van Buren A.L. An exact expression for the lommel-diffraction correction integral. J. Acoust. Soc. Am., 55 (1974), pp. 724-728

[7] B. Zhao, O.A. Basir, G.S. Mittal, Estimation of ultrasound attenuation and dispersion using short time Fourier transform, Ultrasonics, Volume 43, Issue 5, March 2005, Pages 375–381.

The results presented in the figure indicate that despite the pulse echo measurement being more affected by uncertainties, the difference between pulse-echo and through-transmission within the transducer's bandwidth is practically negligible.

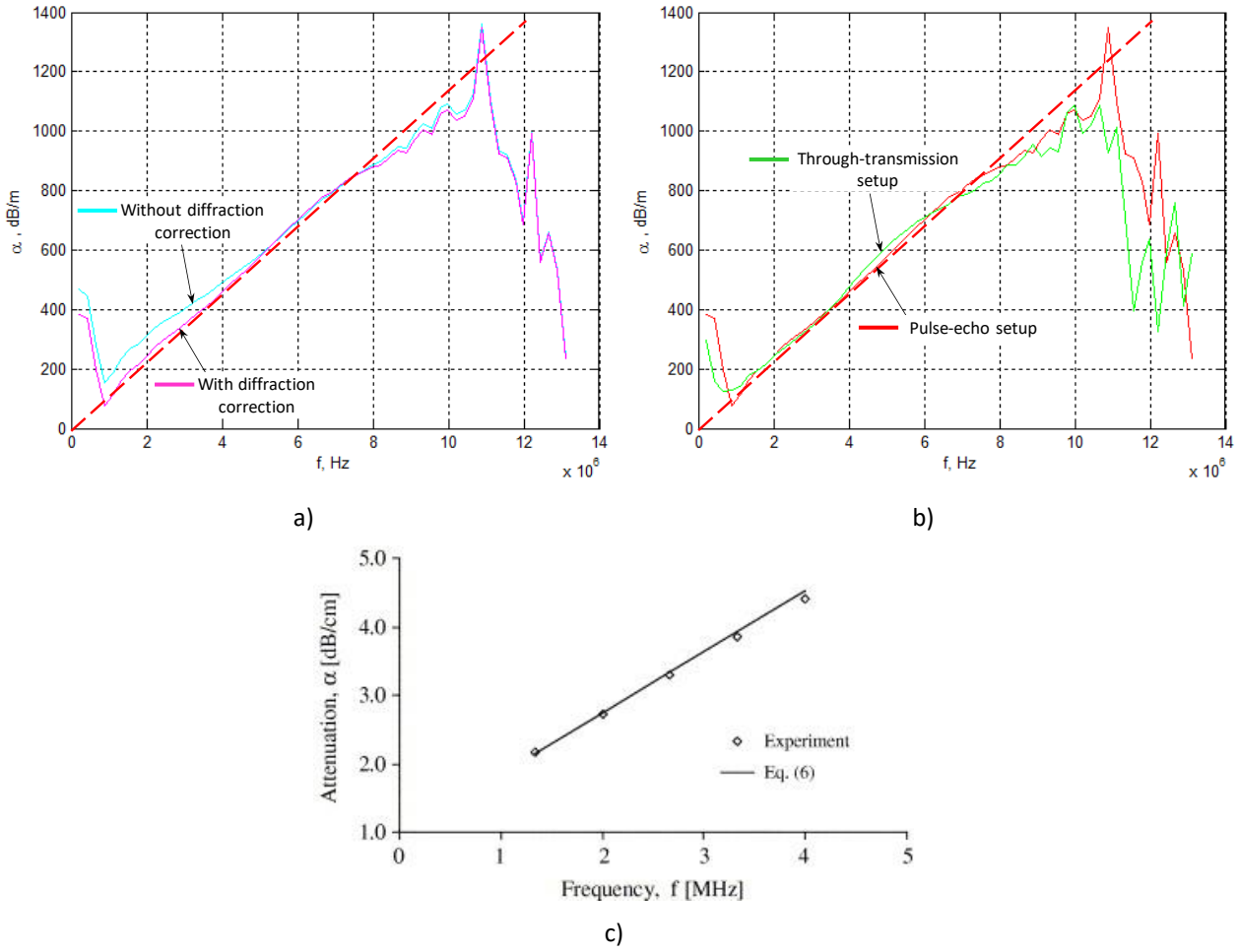

Figure 3-10. Frequency dependent attenuation curves obtained on 20mm plexiglass: pulse-echo measurements with and without diffraction correction (a), comparison between pulse-echo and through-transmission measurements with diffraction correction (b), reference[3] attenuation dependency in plexiglass (c)

3.3.4 Verification results on relevant mock-ups

In this section, average grain size reconstruction results obtained on samples described in section 3.3.1 are presented. For mock-ups 1618-B359-B1, B359-2 and 1618-B359-B3 measurements were taken across the thickness of the sample, stacking mock-ups on top of each other in the immersion tank. A 5MHz flat face probe in pulse-echo arrangement was used as shown in Fig. 3.11a. The average grain size was reconstructed along the measurement line using the technique presented in section 3.1. The estimated average grain size is presented in Fig. 3.15b. From the results it can be estimated that the reconstructed average grain size for samples 1618-B359-B1 and B359-2 corresponds quite well to metallographic analysis (89.2µm and 288µm). The results for sample 1618-B359-B3 show some discrepancies. It can be observed that average grain size is lower at the centre of the mock-up and increases to the edges. This was confirmed with the Cscan of the sample, which is presented in Fig. 3.12. The colour coded back wall amplitude on the Cscan indicates that the magnitude of the reflection signal is higher at the centre of sample, meaning that attenuation at this zone is lower, compared to the zones in close proximity to the edges. This suggests that the mock-up 1618-B359-B3 is heterogeneous, and the reconstructed average grain size will depend on the measurement position.

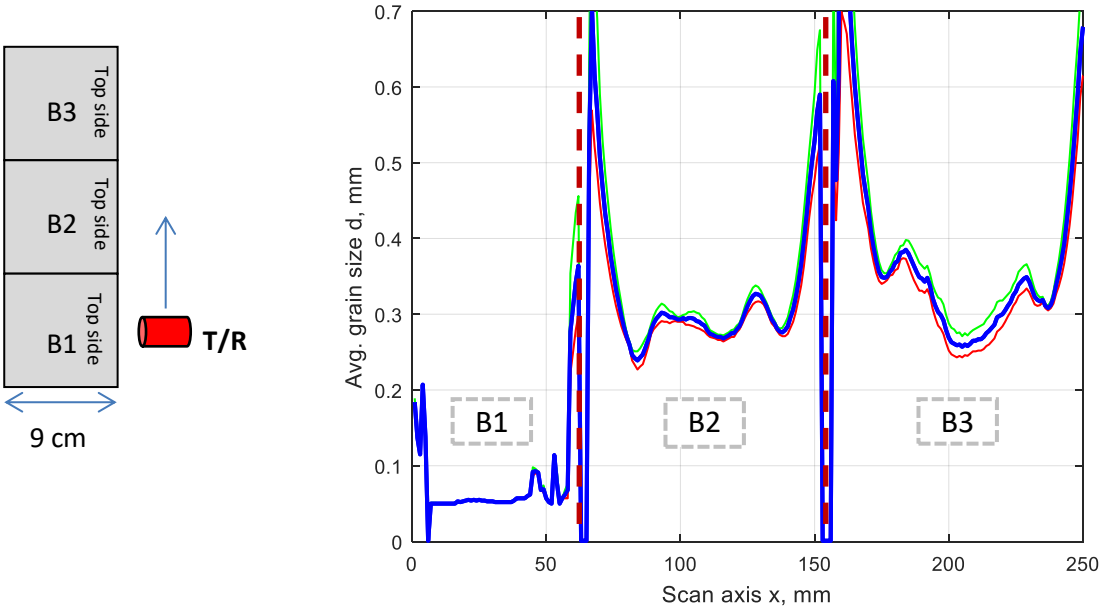

a) b)

Figure 3-11. Attenuation measurement set-up for acquisition of ultrasonic data from 1618-B359-B1, B359-2 and 1618-B359-B3 mock-ups (a) and reconstructed average grain sizes (b)

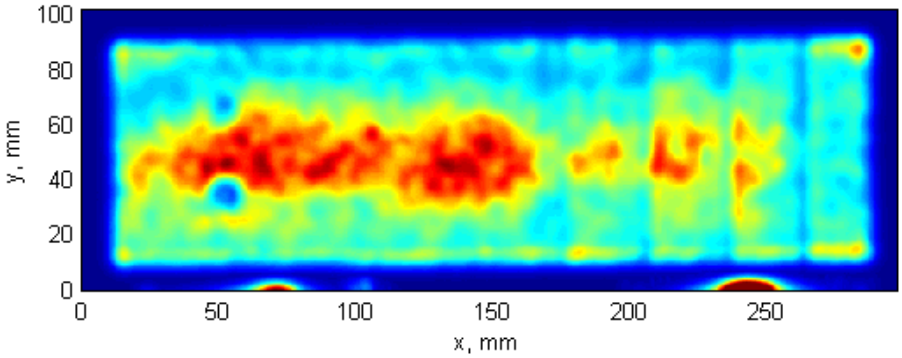

Figure 3-12. Cscan of the back wall reflection of 1618-B359-B3 mock-up

To reconstruct average grain size on the RDIM3 pipe segment, a Cscan of the part of the mock-up was acquired as shown in Fig. 3.13a. Due to its coarse-grained structure, the measurements were taken at 1 MHz, using a flat face probe in pulse-echo arrangement. The outcome of average grain size reconstruction is presented in Fig. 3.13b. The results suggest that reconstructed grain sizes vary in a range of 1.4 mm to 1.9 mm. It will be demonstrated in subsequent chapters that large grains dominate in the attenuation. The investigated structure has fine grain clusters of 300 µm embedded in a matrix of coarse grains. Since the large grains dominate in the attenuation measurement, the reconstructed grain sizes correspond to coarse grains of the structure. The maximum reported grain diameter from metallographic analysis for this RDIM3 mock-up is 2.4 mm.

The measurements for 1591-B359-D2 and 1591-B359-D3 were acquired using 5 MHz probe using pulse-echo probe arrangement. Cscan data was collected by scanning a probe along and across the surface of mock-ups. The reconstructed average grain size map is presented in Fig. 3.14. It can be observed that mock-up 1591-B359-D2 has a quite homogeneous structure. Meanwhile on mock-up 1591-B359-D3 few zones with

increased average grain size can be observed, especially at top right corner. The specific zones corresponding to increased grain sizes were analysed later in this report. In general, both 1591-B359-D2 and 1591-B359-D3 possess similar average grain sizes, which are approximately about 75 µm.

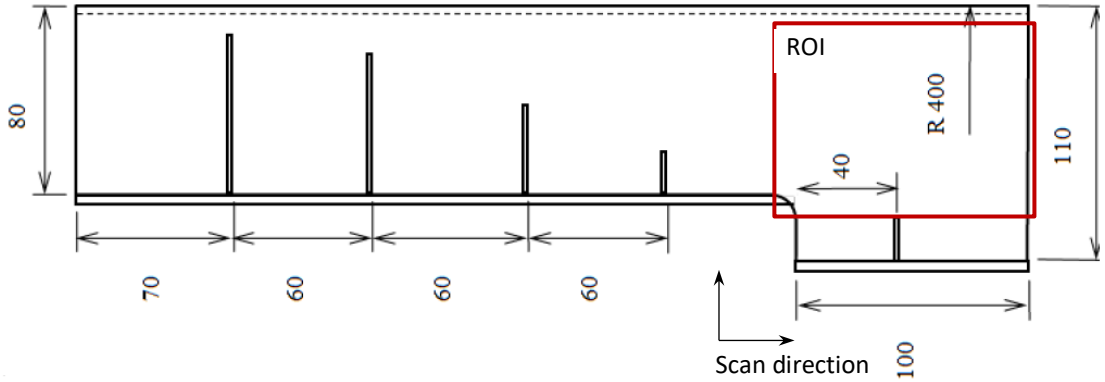

a)

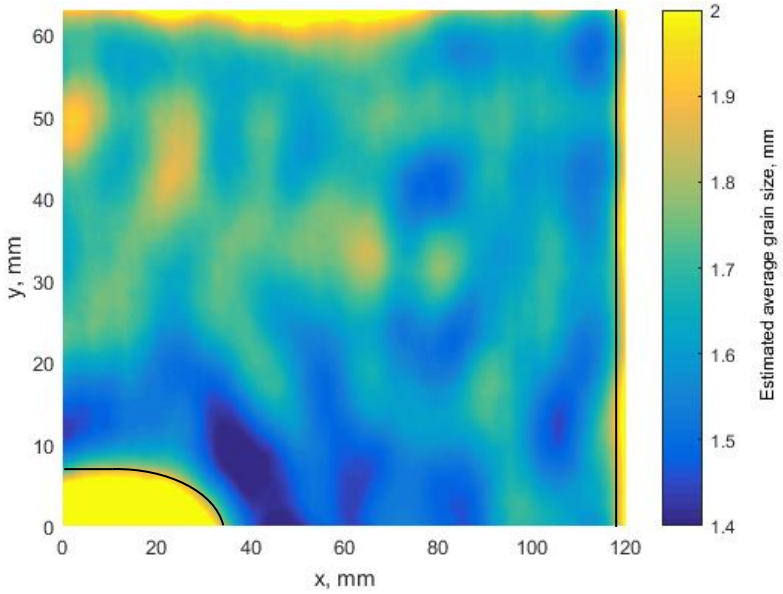

b)

Figure 3-13. Attenuation measurement segment on the RDIM mock-up (a) and reconstructed average grain size (b)

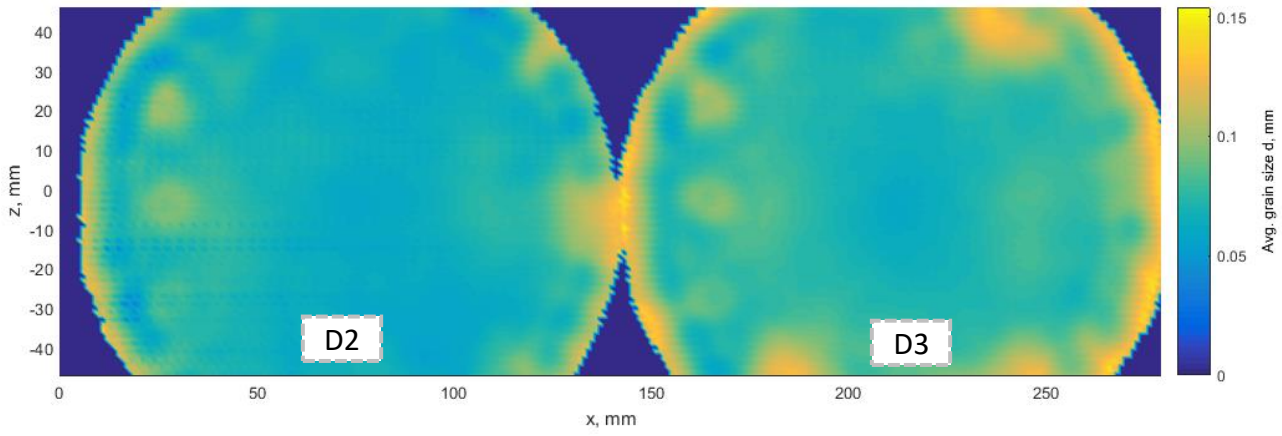

Figure 3-14. Reconstructed average grain size map on mock-ups 1591-B359-D2 and 1591-B359-D3

3.4 Sensitivity analysis

In this section, the sensitivity analysis of the attenuation measurement procedure is conducted. The aim of such analysis is to determine which factors influence the accuracy of attenuation measurements most. The attenuation measurement results obtained on a 36.6 mm steel block with 5 MHz probe were used for this analysis.

In the simplest form, the frequency dependent attenuation can be calculated from the ratio of amplitude spectra of two reflected pulses. However, when transmitting and receiving transducers have a finite size, diffraction introduces some changes to amplitude and phase spectra of the signals. Transmission and reflection coefficients take into account the acoustic impedances of the measurement media and subsequently add a frequency independent shift to the attenuation curve. As a result, in order to get precise attenuation estimations, transmission/reflection coefficients and diffraction has to be taken into the account, where latter has a quite significant effect when measurements are taken in reflection mode. Different components of attenuation curves can be seen in Fig. 3.15. Here the blue curve represents the ratio of the amplitude spectra of two reflected signals, while orange and yellow show diffraction correction (at 100 mm) and transmission/reflection coefficients. The sum all three abovementioned curves leads to the final attenuation estimation (green). It can be observed that diffraction correction is frequency dependent, thus it changes the slope of the attenuation curve. Meanwhile the transmission/reflection coefficients have no frequency dependence, hence they change vertical offset of the attenuation curve.

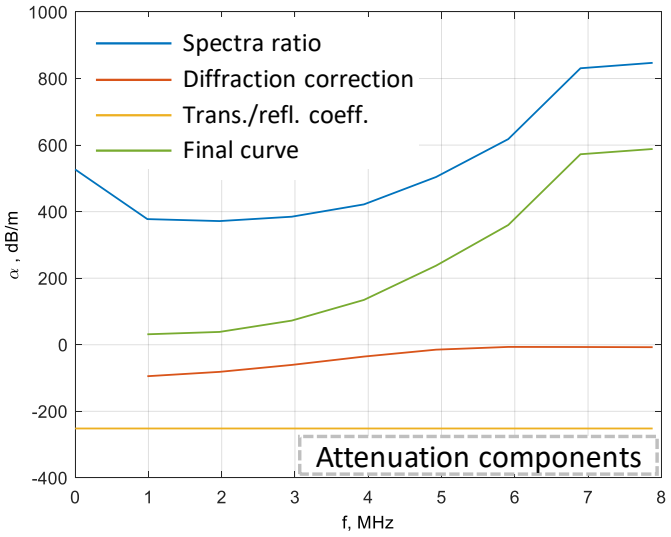

Figure 3-15. Illustration of different components of attenuation curve

During the sensitivity analysis presented in this section, various parameters were changed to observe their impact on the final attenuation curve. The attenuation calculation procedure as described in section 3.3 takes into consideration different parameters related to probe, material and experimental arrangement. The following parameters can be emphasized, which may have a significant impact on attenuation: material velocity, material density, probe diameter, sample thickness and probe distance to sample. Each parameter was altered within a specific range and the attenuation curve was calculated according to the equations presented in section 3.3. The results are shown in Fig. 3.16.

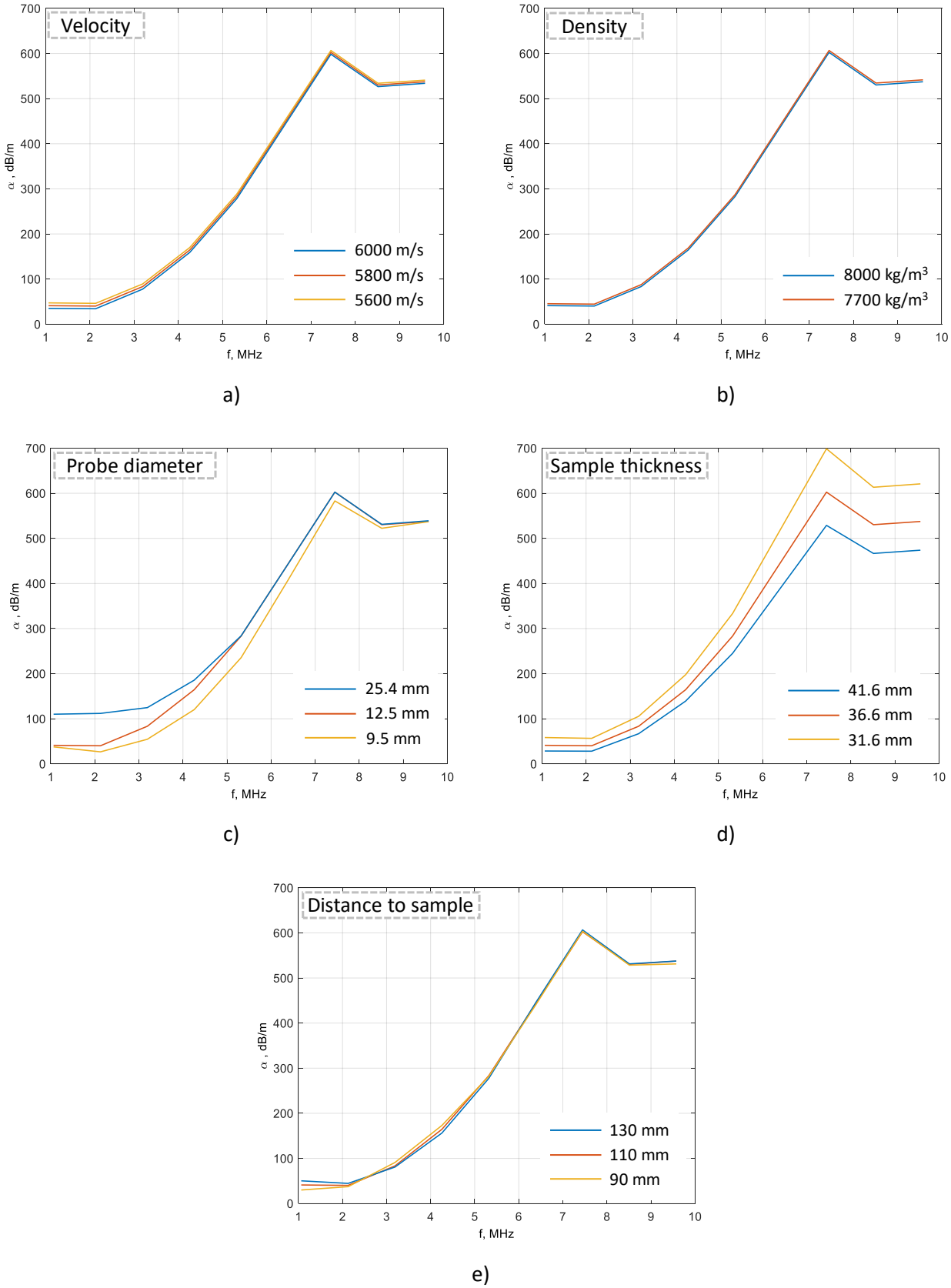

Figure 3-16. Attenuation curves calculated using variable velocity (a), density (b), probe diameter (c), sample thickness (d) and distance to sample (c)

The results presented above indicate that parameters that are included in diffraction correction, such as probe diameter and sample thickness, influence attenuation estimation most. It is known that diffraction

correction has negligible effect on phase spectra of received signal and amplitude spectra of transmitter signals. Probe diameter is usually well known, while the sample thickness problem can be eliminated employing the phase spectrum. However, such an approach requires both transmission and reflection signals.

4 Grain size estimation based on TPCF

The modelling performed by ICL revealed that at certain circumstances, there is a possibility that two distributions, one with a large mean and small standard deviation-to-mean ratio and the other one with a small mean and large standard deviation-to-mean ratio, have similar attenuation against frequency curves. This makes evaluation of mean grain size from attenuation non-unique.

Grain size can be described with a two point correlation function TPCF, which shows probability of two random points to be located in same grain. It is often approximated with an exponential exp(-r/a), where *a* is called the linear correlation length. TPCF allow to take into consideration grain size distribution, although it requires to relate the grain size distribution to the TPCF. This section is a summary of the published paper[1], where mainly the contributions from ICL and EDF to WP2, T2.3 are presented.

4.1 Mock-up and model descriptions

4.1.1 Attenuation measurement

The mock-up used in this section is one out of six sections with about 135 mm diameter and 100 mm height which were cut out of a cylindrical cast Inconel 600 slab (EDF reference 1591-B359-D3). The sections underwent heat treatment with the effect of increasing grain size through the merging of smaller grains during the heating and subsequent annealing cycle. The mock-up is assumed to be homogeneous in a macroscopic sense, with approximately equiaxed grains and no texture. Further, it does not exhibit a layered structure with different grain sizes.

Attenuation measurements for mock-up D3 were carried out according to the procedure described in section 3.3. Measurements were taken using both pulse-echo and through transmission set-ups. Maps of attenuation coefficients $\alpha_{PE}(f)$ and $\alpha_{TT}(f)$ at f=5 MHz are presented in Fig. 4.1. On the left-hand side of each map, the footprints of three flat-bottomed holes, purposely manufactured in the mock-up, can be observed. Three areas corresponding to distinctly different attenuation levels were identified from the attenuation map. The zones are referred to as “Zone 1”, “Zone 2” and “Zone 3” and their locations are marked in Fig. 4.1. The circles around each zone show the footprint of the probe at each scanning position. The subsequent sections of this deliverable use a single PE attenuation curve for each zone (taken at the centre of the circles in Fig. 4.1: (x_1=73 mm, y_1=47 mm) - Zone 1; (x_2=95 mm, y_2=87 mm) - Zone 2; (x_3=105 mm, y_3 =47 mm) - Zone 3).

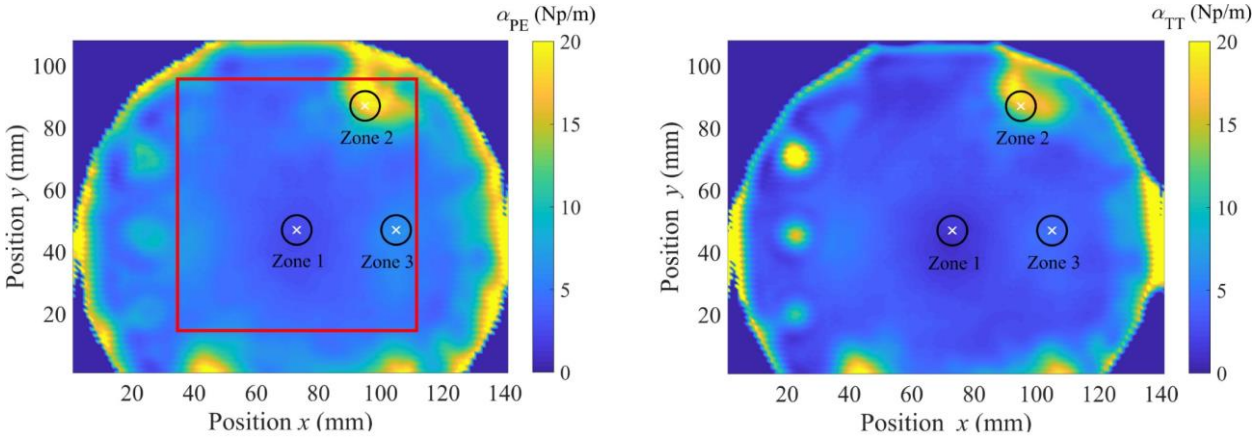

a) b)

Figure 4-1. Attenuation coefficients (a) $\alpha_{PE}(f)$ and (b) $\alpha_{TT}(f)$ at the central frequency (5 MHz) of the probe

To demonstrate the range of attenuation in the specimen, we plotted the results for all points within the rectangular area marked in Fig. 4.1(a), overlaid with the curves corresponding to the centres of the chosen

zones defined above, in Fig. 4.2, where the curves close to the upper bound were measured close to the mock-up edge so are affected by the edge reflections.

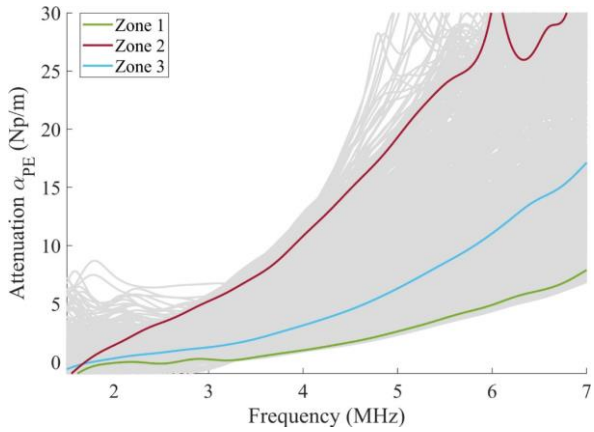

Figure 4-2. Attenuation at the centres of the three selected zones; grey lines represent the attenuation at all points within the rectangular area marked in Fig. 4.1(a)

4.1.2 Mock-up D3 characterisation

The metallographic analysis was carried out for 1591-B359-D3 mock-up at three zones referred as “Zone 1”, “Zone 2” and “Zone 3” by first polishing the surface to be analysed with increasingly fine sanding paper, then immersing the part for a certain time in aqua regia, a concentrated mixture of nictric and hydrochloric acids. This acid attack reveals the grain structure, which would then be investigated under a microscope, if the part was small enough. In this case, a thin layer of liquid plastic was applied on the three regions (“Zone 1”, “Zone 2” and “Zone 3)”, which was removed after solidification and subsequently analysed. The contrast of the grain boundaries revealed to be too low to produce a binary image. The microscope scans were therefore printed in A3 format, and the boundaries were manually drawn upon a superimposed transparency film. This film was then scanned and the resulting image was fed into the processing workflow. The scanned films for the three zones are shown in Fig. 4.3(a), (c) and (e).

Each characterisation presented in figure above covered an area of approximately 1.35 mm×0.96 mm. After binarisation, all images were processed to remove artefacts and close some open grain boundaries. The final step was the segmentation which yielded a numbered list of grains and their geometric properties, including size. We assumed the standard definition of grain size, understood as the diameter of a circle of an area equal to that of the 2D grain in the metallographic image (equivalent diameter). The histograms of the equivalent diameters for the three zones are shown in Fig. 4.3(b), (d) and (f), together with the probability density functions of their log-normal fits. The means and standard deviation-to-mean ratios of the fitted distributions are (51.9 µm, 0.74), (66.8 µm, 0.84) and (60.1 µm, 0.64) for “Zone 1”, “Zone 2” and “Zone 3”, respectively.

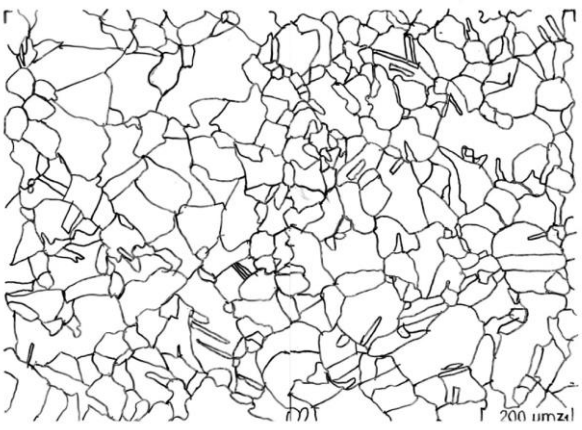

a)

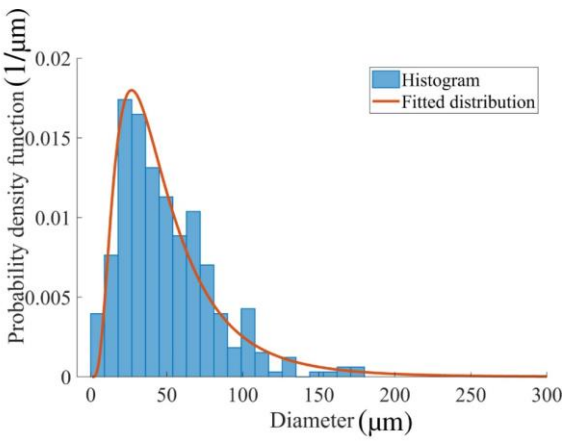

b)

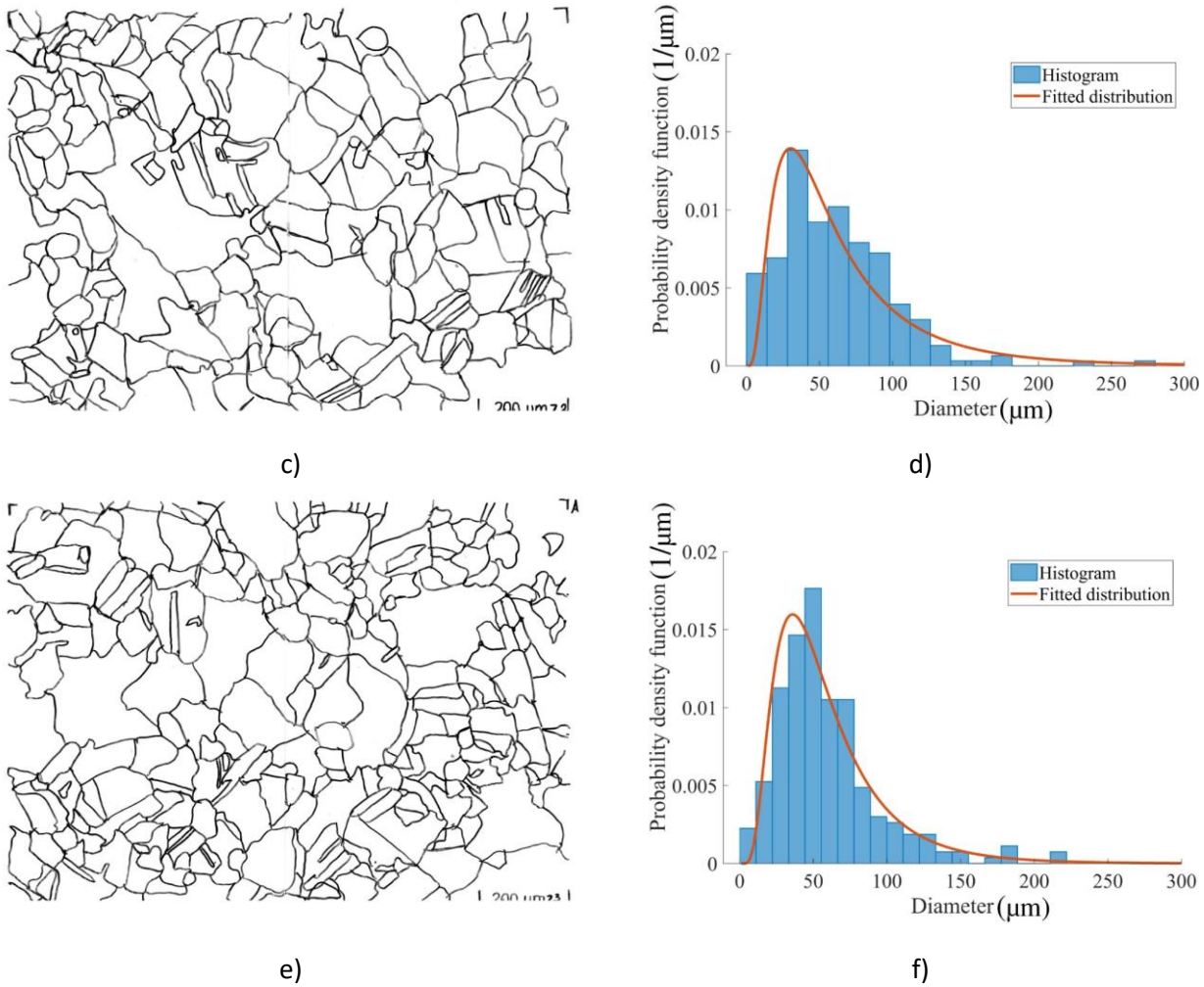

Figure 4-3. Metallographies of (a) Zone 1, (c) Zone 2 and (e) Zone 3, with histograms of the equivalent grain diameters and the probability density functions of their log-normal fits for: (b) Zone 1, (d) Zone 2 and (f) Zone 3

4.1.3 FE model description

Numerical synthetic microstructures used to investigate the effect of grain statistics on attenuation were generated in *Neper* using a log-normal distribution. Based on the examination of the mock-up we chose the ranges of distribution parameters for investigation. The mean grain size, denoted by κ, and the standard deviation-to-mean ratio of the grain size, denoted by $\overline{\overline{D}}$, ranged from 45 µm to 70 µm and from 0.2 to 0.6, respectively. For the sake of brevity, we describe a grain size distribution as ($\overline{\overline{D}}$, κ). For example, a grain size distribution of (50 µm, 0.2) means that the mean grain size is 50 µm and the standard deviation is 0.2×50 µm=10 µm. The geometry of each model was a cuboid, with the wave propagating in the direction of the longest side Fig. 4.4. The dimensions of the models were ($20 \times \overline{\overline{D}}, 20 \times \overline{\overline{D}}, 200 \times \overline{\overline{D}}$). The models used regular structured meshes. Linear hexahedral elements (3D 8-node brick, of the C3D8 type) with an edge length of $\overline{\overline{D}}/20$ were chosen. All the models were composed of Inconel 600 with cubic symmetry. The elastic constants (C_{11}, C_{12}, C_{44}) and density of the crystal were (234.6 GPa, 145.4 GPa, 126.2 GPa) and 8290 kg/m^3, respectively. To simulate the wave propagation, highly efficient GPU-based FE solver Pogo was used. A schematic diagram of the model used to calculate the attenuation is shown in Fig. 4.4. Symmetry boundary conditions used on the surfaces parallel to the *z*-axis made the model equivalent to being infinitely wide with repeating grain structures. All nodes on the *x*–*y* plane, shown as the red dots in Fig. 4.4, acted as transmitters exciting a plane wave propagating in the direction. The nodes on the opposite surface, shown as the blue dots, acted as receivers. The coherent attenuation coefficient α was obtained by comparing the spatial average of the first wave packets received by the receivers to the spatial average of the responses over the

transmitting nodes in the frequency domain. A 3-cycle Hann-windowed tone burst with centre frequencies of 6, 8, 10, 12 and 14 MHz was the excitation signal, covering the range from 6 to 14 MHz.

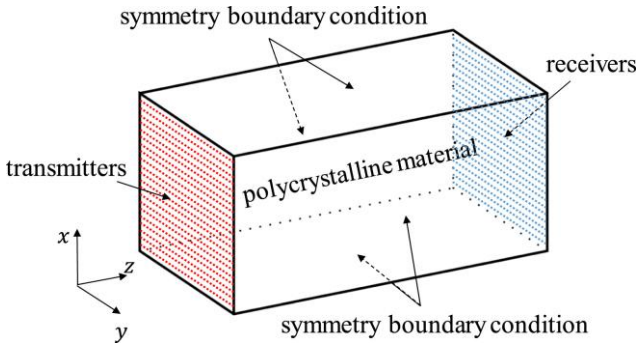

Figure 4-4. A schematic diagram of the model used for calculating attenuation

4.2 Effect of grain size distribution on attenuation

In this section, the effect of different grain distribution parameters, such as standard deviation to mean ratio, mean grain size, to the attenuation are considered. First, the attenuation against different standard deviation to mean ratio κ with different grain sizes 50µm, 60µm and 70µm at 10MHz are presented in Fig. 4.5. It can be observed that attenuation increases with increase of standard deviation to mean ratio. This indicates that as κ increases, the maximum grain size increases as the distribution becomes more skewed. Consequently, the number of total grains in the considered volume reduces. Hence, the large grains start to dominate, resulting in the rise of attenuation.

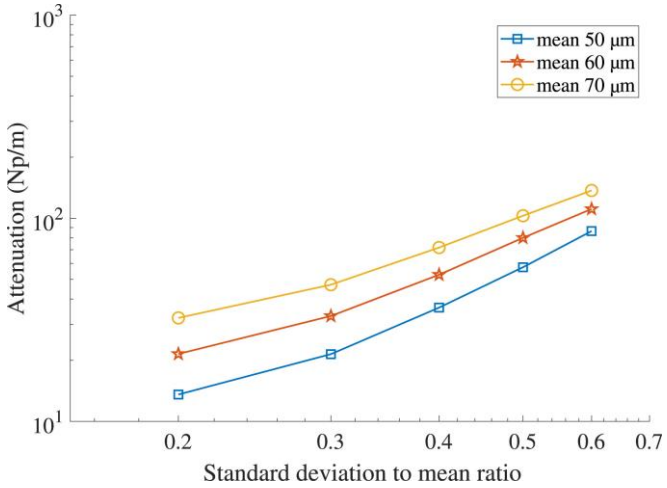

Figure 4-5. Attenuation against the standard deviation-to-mean ratio at 10 MHz with different mean grain sizes

To explore attenuation dependence on mean grain size at different standard deviation to mean rations, three κ values (0.2, 0.4 and 0.6) were considered and for each ratio, mean grain size in the range of 45 to 70 µm was estimated. From simulated time traces, attenuation at 10 MHz for all combinations of grain size distributions were calculated and presented in Fig. 4.6a. Additionally, the results at κ=0.4 and frequencies of 6, 10 and 14 MHz can be seen in Fig. 4.6b.

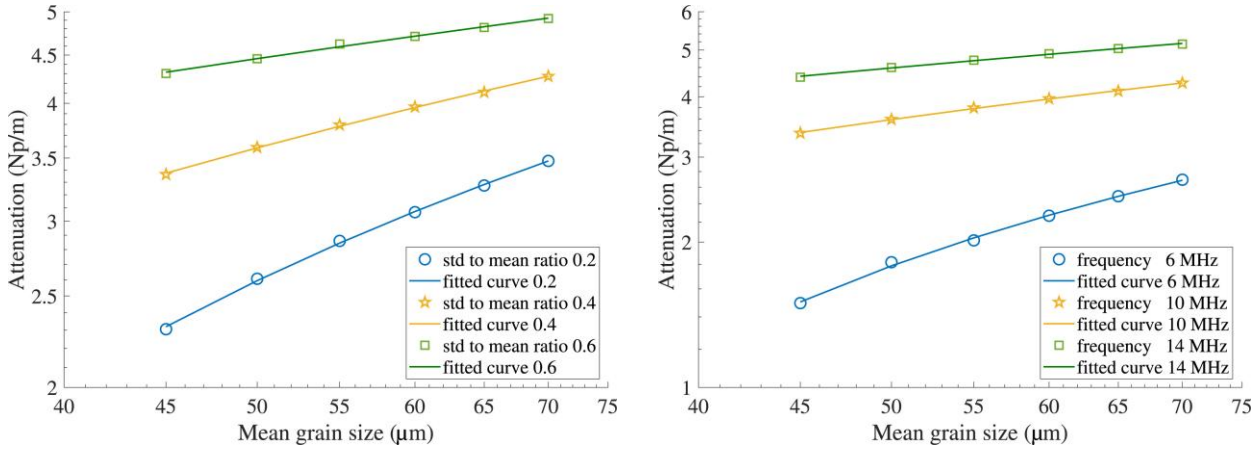

a) b)

Figure 4-6. Attenuation vs mean grain size: standard deviation-to-mean ratios of 0.2, 0.4 and 0.6, at 10 MHz (a), standard deviation-to-mean ratio of 0.4, at 6, 10 and 14 MHz (b)

The results presented above indicate that the attenuation increases with mean grain size for all cases, but less rapidly for models with a higher standard deviation-to-mean ratio or higher frequencies. Attenuation against frequency curves with different standard deviation-to-mean ratios of grain size are plotted in Fig. 4.7. The attenuation increases with frequency for all cases, but less rapidly for larger standard deviation-to-mean ratios. The fitted power of the frequency dependence of attenuation is listed in Table 4.1. Two frequency ranges, 6–7 MHz and 13–14 MHz, are used for fitting each of the five curves corresponding to different standard deviation-to-mean ratios. Table 4.1 shows that, when increasing from 0.2 to 0.6, the power of frequency dependence reduces from 4.13 to 3.09 over the frequency range of 6–7 MHz, and from 3.56 to 2.06 over the frequency range of 13–14 MHz. It is worth noting that the power 4.13, which is larger than 4, could be due to the coarse element used for calculation. At a higher frequency, the power drops more rapidly. The decrease of the power of frequency dependence indicates that the scattering is out of the Rayleigh region, although the wavelength-to-mean grain size ratio is much greater than 1.

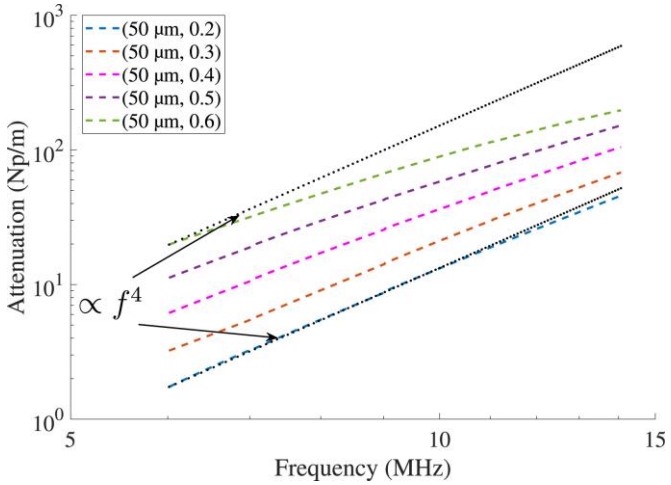

Figure 4-7. Frequency dependence of attenuation obtained with a mean grain size of 50 μm and standard deviation-to-mean ratios from 0.2 to 0.6

Table 4-1. Fitted power of frequency dependence of attenuation; std stands for standard deviation.

Mean (μm)	*std* (μm)	*std to mean ratio*	*Fitted power (6–7 MHz)*	*Fitted power (13–14 MHz)*
50	10	0.2	4.13	3.56
50	15	0.3	3.45	3.27

Mean (µm)	*std* (µm)	*std to mean ratio*	*Fitted power (6–7 MHz)*	*Fitted power (13–14 MHz)*
50	20	0.4	3.56	2.98
50	25	0.5	3.42	2.71
50	30	0.6	3.09	2.06

The results presented in this section suggests that increasing the mean and standard deviation-to-mean ratio of the grain diameter both increase the attenuation and decrease the frequency dependence power of attenuation. Therefore, there is a possibility that two distributions, one with a large mean and small standard deviation-to-mean ratio and the other one with a small mean and large standard deviation-to-mean ratio, have similar attenuation against frequency curves, which is demonstrated in Fig. 4.8. The models with distributions of (45 µm, 0.6) and (70 µm, 0.4) have very similar attenuation curves, higher than the other set of examples of (50 µm, 0.3) and (60 µm, 0.2), which are also very close to each other. This highlights a big challenge for determining mean grain size from an ultrasonic attenuation measurement.

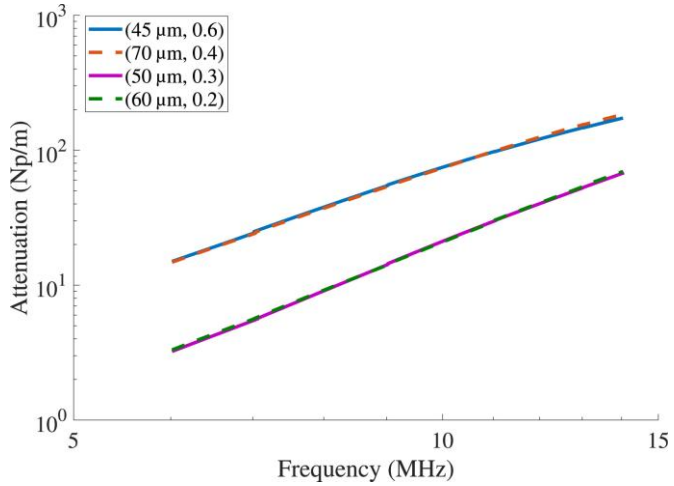

Figure 4-8. Examples of similar attenuation curves obtained with different grain size distributions

4.3 Estimation of grain statistics based on TPCF

In order to elucidate the limitations of grain size estimation based on attenuation measurement, we employ the second-order approximation[8], which uses a TPCF to describe the grain statistics and to predict the attenuation. As mentioned in previous chapters, the TPCF is often modelled by an exponential function, $\exp(-r/a)$, where a is the linear correlation length. While average grain size is the most common metric used in the industry, in this section we consider the linear correlation length as the target for the inverse problem.

Three attenuation curves, measured at the centres of the different locations, 'Zone 1', 'Zone 2' and 'Zone 3', were used to evaluate the grain size. Locations of the three zones can be found in Fig. 4.1. A family of theoretical curves were first produced using the second-order approximation model with a set of linear correlation lengths. Then, the attenuation measurements were compared with the theoretical curves. The correlation length offering the best match was identified as the target value characterising the microstructure at each location. The values identified from the attenuation measurement were compared with the

[8] Sha G., Huang M., Lowe M., Rokhlin S. Attenuation and velocity of elastic waves in polycrystals with generally anisotropic grains: Analytic and numerical modelling. J. Acoust. Soc. Am., 147 (2020), pp. 2442-2465

correlation lengths obtained by fitting single exponentials to the TPCFs calculated from the metallography images shown in Fig. 4.3.

The comparison of the linear correlation lengths calculated from the metallography images and estimated from the attenuation measurements is gathered in Table 4.2. Zone 1 and Zone 3 show good agreement, with the evaluation from ultrasonic measurements being 10%–20% lower than the metrics obtained from metallography.

Table 4-2. Linear correlation lengths calculated from the metallography images and estimated from the attenuation measurements.

Zone number	*From metallography*	*From attenuation*	*Relative error, %*
Zone 1	33.6	27.8	17
Zone 2	47.6	66.7	–40
Zone 3	45.0	38.8	14

However, the comparison of Zone 2 shows a larger discrepancy, and the trend is opposite to the others, i.e. the estimation from attenuation is higher than the reference from the metallography image. This different trend may be explained by Fig. 4.9 and Fig. 4.1a, which show the measured TPCFs and fitted TPCFs for the three zones and the attenuation measured across the mock-up at 5 MHz, respectively. It can be seen that, for Zone 2, a single exponential which gives the best fit underestimates the fraction of large grains, which dominate the attenuation. On the other hand, for the other zones, there is a relatively good agreement between the measured and the fitted TPCFs. In addition, Fig. 4.1a suggests that the grain size distribution is relatively uniform near Zone 1 and Zone 3 but it varies considerably around Zone 2. The bright yellow spot near Zone 2 represents a high attenuation and suggests there are large grains in that area. Therefore, the small metallography fingerprint taken in Zone 2 might not be able to reflect the microstructure seen by the transducer. Hence, the linear correlation length obtained from the metallography very likely underestimates the grain size. We also note that our work assumes equiaxed grains which may not always be satisfied, in particular close to the edges. Although there is no evidence that columnar grains or texture are present in this sample, they remain a factor to consider.

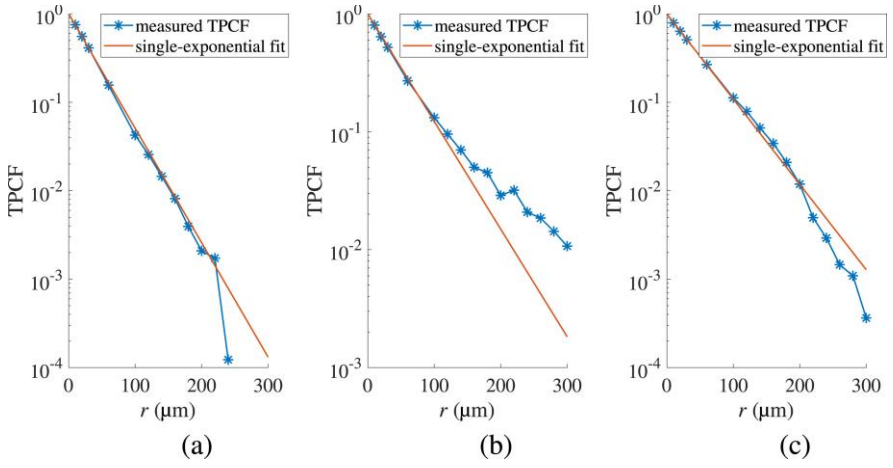

Figure 4-9. Measured TPCFs of (a) Zone 1, (b) Zone 2 and (c) Zone 3 and their single-exponential fits

The linear correlation length can be used as a metric to quantify to what extent the microstructure of a component under inspection is similar to the microstructure of the mock-ups on which the inspection method was qualified. If the microstructure of the actual component under inspection exhibits a larger average grain size, a degradation of the inspection performance would be expected. On the other hand, a

smaller average grain size should increase the performance margin. With this in mind, a logical next step would be to apply the linear correlation length metric to an actual cast component mock-up in order to produce an extended cartography covering the entire inspection surface. One might expect to find more significant local grain size variations in a component mock-up, which the linear correlation length cartography should reflect. Implanting defects on regions identified as penalising due to a coarser grain structure should then allow to determine the actual inspection performance degradation, and to establish acceptable margins.

5 Conclusions

In this deliverable, the investigation how the average grain size and statistical distribution of grains affects the attenuation of ultrasound in cast components was presented. Following messages can be taken from this research:

1. Attenuation measurement can be considered as a pragmatic choice for evaluation of the grain statistics and assessment of the inspectability of the components using a given qualified procedure.
2. The average grain size reconstruction based on the Stanke-Kino model can be used as rough indicative average grain size evaluation metric, even considering underlying significant assumptions of cubic symmetry, scattering at grain boundaries, distribution and shape of scatterers included in the model. It was demonstrated with the synthetic microstructure models and experiments, that such estimation provides practicable and reasonable average grain size estimation accuracy.
3. There is a possibility that two distributions, one with a large mean and small standard deviation-to-mean ratio and the other one with a small mean and large standard deviation-to-mean ratio, have similar attenuation against frequency curves leading to non-uniqueness of the average grain size estimation. Due to such reason, the linear correlation length was suggested as more robust and widespread measure non affected by non-uniqueness. It was found that a single exponential fit may underestimate the areas with large grains as these quite essentially dominate the measured attenuation. The other cases demonstrated reasonable agreement between the TPCF calculated from the attenuation and the metallography.
4. While ultrasound is sensitive to material grain morphology both in its propagation and in its back-scattering, this deliverable focused on the attenuation phenomenon only. The backscatter analysis of the mock-ups from the Advise repository yielded to the inconclusive results which may be related to the particular grain structures used. Hence, the backscatter analysis remains the subject of current and future work, while the obtained results were omitted from this report.

6 Annex I: Procedure to calculate average grain size

The assessment of grain size is performed in the following steps:

1. The Stanke-Kino curve (Fig.6.1) for selected type of material is modified in order to obtain dependencies of attenuation versus frequency for particular size of grain. In Fig.6.1 by *a* is denoted grain size; α_L is the attenuation longitudinal waves; k_L is the wavenumber. As the wavenumber is defined by $k_L = \frac{2\pi}{\lambda} = \frac{2\pi}{c} \cdot f$, where *c* is the ultrasound velocity and *f* is the frequency. So, *x* axis of Stanke-Kino curve $k_L a$ can be transformed by multiplying it with $\frac{c}{2\pi}$. It means $k_L \cdot a \cdot \frac{c}{2\pi} = f \cdot a$.
2. In case of known ultrasound velocity *c* the set of dependencies attenuation versus frequency corresponding to different diameter of grain $\alpha_L(f, a_n)$ can be created dividing vertical and horizontal axes by grain size a_n, where $n = 1 \div N$; *N* is the total number of grain sizes used.
   In Fig.6.2 such set corresponding to grain size 0.1, 0.2, …, 1.0mm is presented. In the proposed method this set is generated with smaller step 0.001mm and in wider dimension ranges $a_n = [0.001 \div 7]$ mm. In general, these dependencies enable to determine what attenuation at particular frequency can be expected in the case of particular size of metal grain.

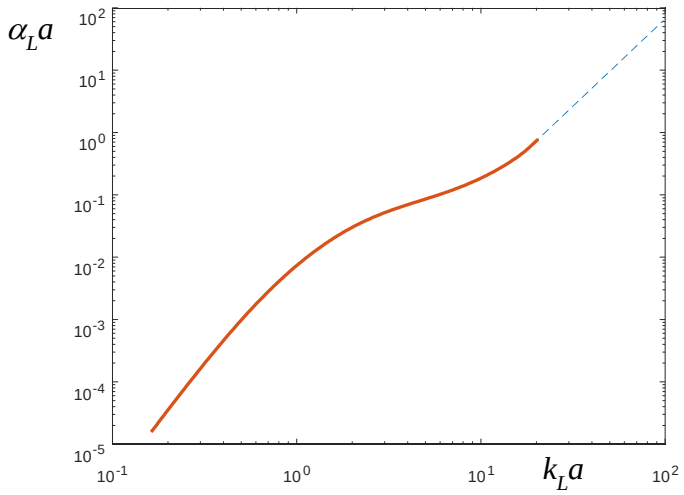

Figure 6-1. The Stanke-Kino curve for Inconel (solid red line) and extrapolation (blue dashed line)

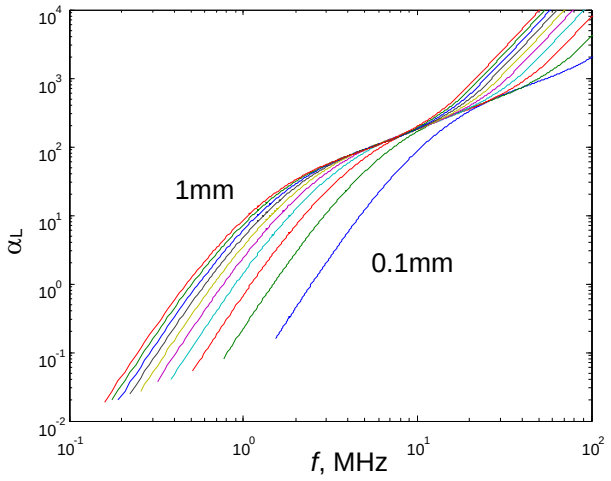

Figure 6-2. Modified Stanke-Kino curves: attenuation versus frequency in the case of grain size 0.1, 0.2, …, 1.0mm

3. Experimentally measured attenuation $a_{\exp}(f)$ is compared with the set of Stanke-Kino curves modified defined in the step 2 and by determining optimal fit the estimation of grain size is obtained:

$$a_{est} = \arg\left\{ \min_{a_n} \left[\left(\lg(\alpha_L(f, a_n)) - \lg(a_{\exp}(f)) \right)^2 \right] \right\}. \quad (6.1)$$

   Example of such fitting is presented in Fig.6.3. In this particular case the best fit corresponds to 0.053mm mean grain size.

4. If step 3 is repeated for the set of experimentally measured frequency dependent attenuation in particular area of sample the variations or distribution of the mean grain size can be obtained in the form of C-scan.

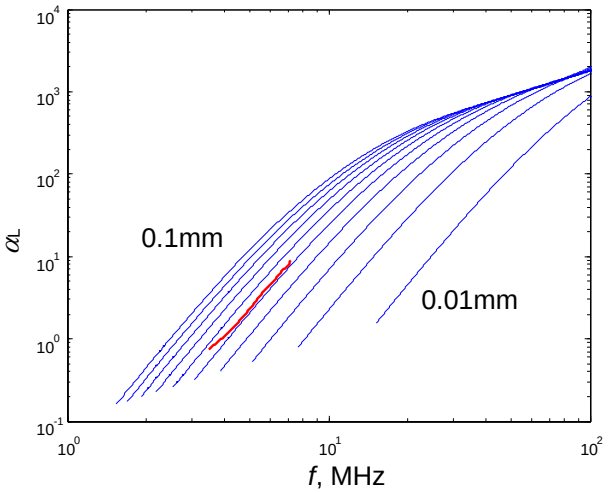

Figure 6-3. Illustration of fitting procedure: set of modified Stanke-Kino curves (blue); experimentally measured frequency dependent attenuation (red)

To illustrate the principle of average grain size estimation, assume that B-scan data was collected on the sample by scanning transducer along one line. At each measurement position along the line, the attenuation can be estimated from either reflected or transmitted signals. Applying the abovementioned technique, the average grain size can be reconstructed at each measurement position. Example of such reconstruction is presented in Fig. 6.4a. Each average grain size estimation corresponds to some minima in cost function, which for single point at red dashed line is illustrated in Fig. 6.4b. It can be observed, that cost function shows quite unambiguous minima, corresponding to 164µm. Similarly, the average grain size can be reconstructed taking 2D measurements in a form of cartography.

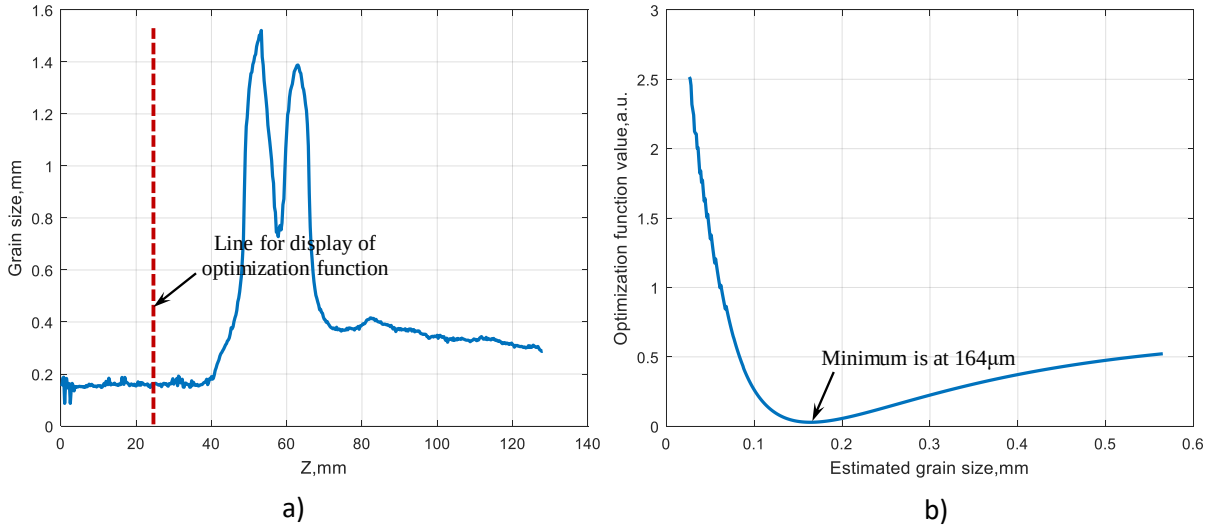

Figure 6-4. Example of reconstructed average grain size along single measurement line (a), cost function at the position corresponding to red dashed line (b)

7 Annex II: Schematic drawings of representative mock-ups

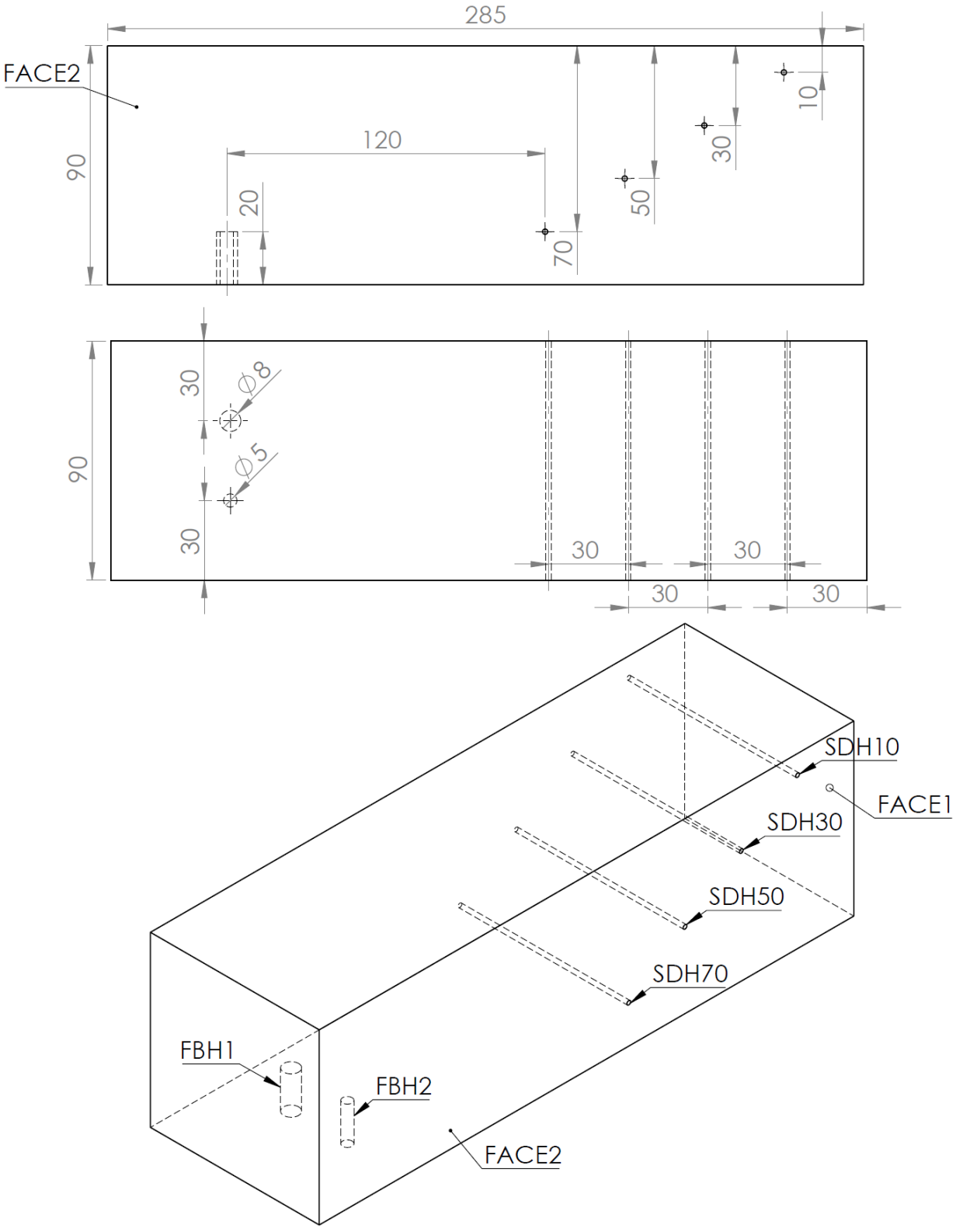

Figure 7-1. The sketch of the mock-ups 1618-B359-B1, B359-2 and 1618-B359-B3

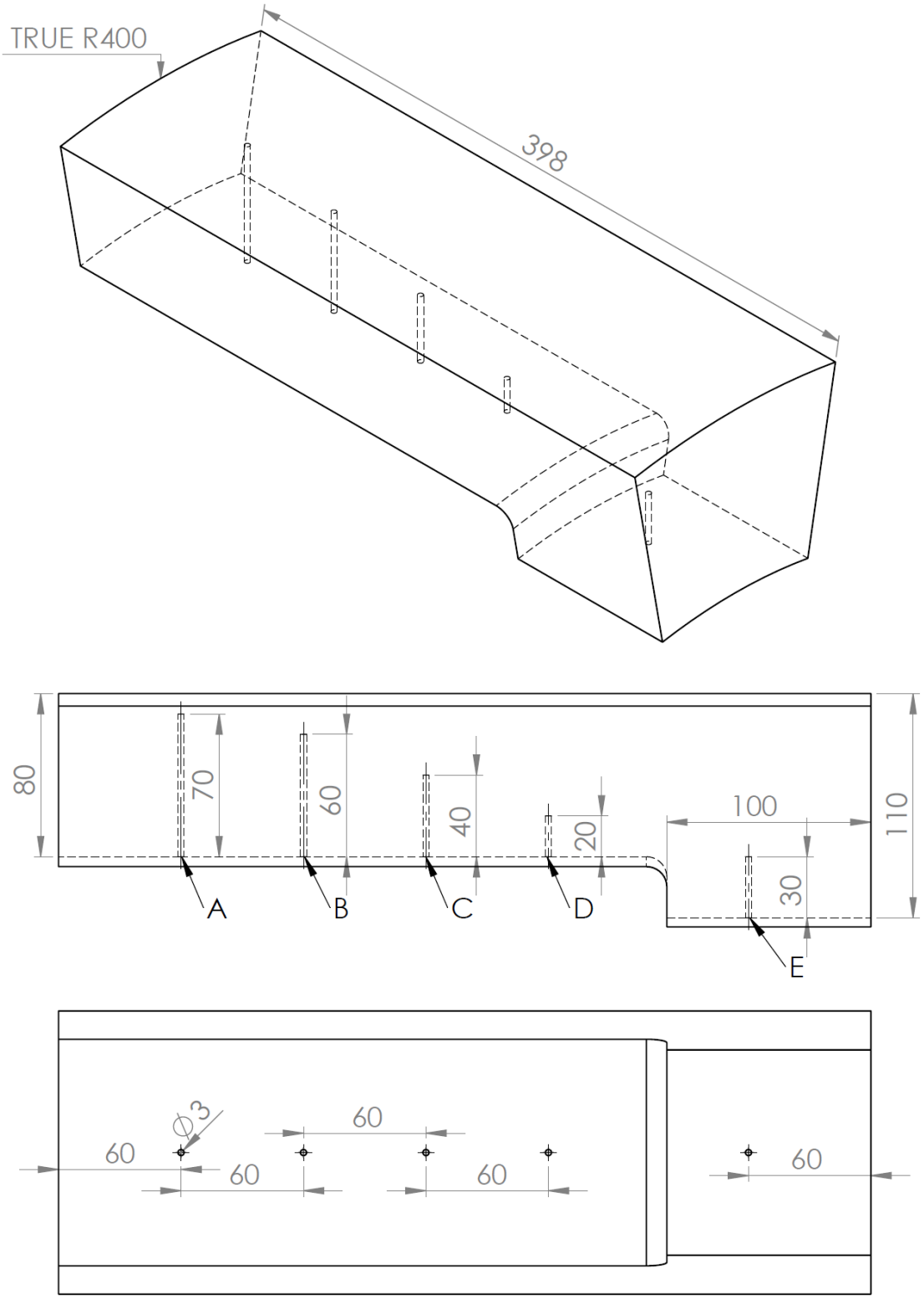

Figure 7-2. The sketch of the mock-up RDIM3

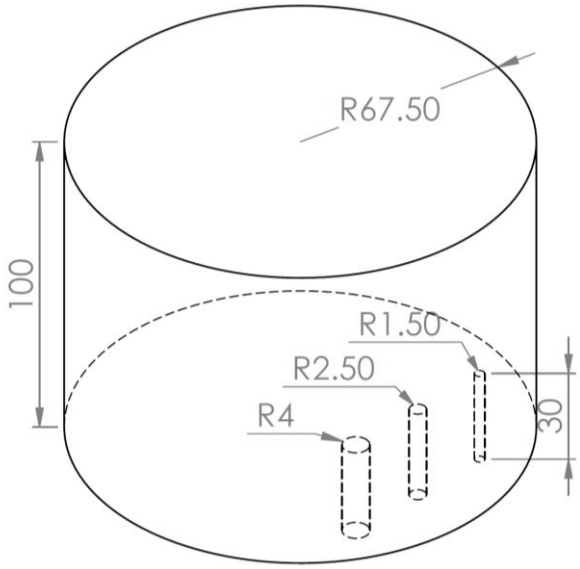

Figure 7-3. The sketch of the mock-up 1591-B359-D2, 1591-B359-D3, 1591-B359-D4